Hybrid Perovskite Phase Transition and Its Ionic, Electrical and Optical Properties

Md Nadim Ferdous Hoque[1], Nazifah Islam[1], Kai Zhu[2], Zhaoyang Fan[1]

[1] Electrical & Computer Engineering, Texas Tech University, Lubbock, Texas, United States
[2] National Renewable Energy Laboratory, Golden, Colorado, United States

ABSTRACT

Hybrid perovskite solar cells (PSCs) under normal operation will reach a temperature above ~ 60 °C, across the tetragonal-cubic structural phase transition of methylammonium lead iodide ($MAPbI_3$). Whether the structural phase transition could result in dramatic changes of ionic, electrical and optical properties that may further impact the PSC performances should be studied. Herein, we report a structural phase transition temperature of $MAPbI_3$ thin film at ~ 55 °C, but a striking contrast occurred at ~ 45 °C in the ionic and electrical properties of $MAPbI_3$ due to a change of the ion activation energy from 0.7 eV to 0.5 eV. The optical properties exhibited no sharp transition except for the steady increase of the bandgap with temperature. It was also observed that the activation energy for ionic migration steadily increased with increased grain sizes, and reduction of the grain boundary density reduced the ionic migration.

INTRODUCTION

In spite of recent tremendous progress of PSCs leading toward efficiency over 22%, there are lots of issues regarding long term stability of these solar cells [1]. Moreover, $MAPbI_3$ has a tetragonal-cubic phase transition temperature in the range of 42-57 °C [2]. This transition needs to be addressed, since on a hot summer day a device can easily reach this temperature [3]. Specifically, electronic, and ionic migration characteristics under normal solar cell operating conditions have drawn special attention [4-8]. Ionic migration is attributed to the hysteresis phenomenon as well as gradual degradation of $MAPbI_3$ to MA^+ and PbI_2, which becomes more prominent under illumination [6]. Moreover, recent development in surface characterization by different types of atomic force microscopy (AFM) has enabled more in-depth research at nanoscale for the charge transport mechanisms [9, 10]. However, there is still missing links between grain size and the ionic activation energy for the intrinsic $MAPbI_3$ films across the phase transition.

In this work, we have focused on the phase transition property of $MAPbI_3$. Structural, electrical and optical measurements were conducted to characterize the tetragonal-cubic structural phase transition and the related ionic/electrical and optical property changes. We also address the grain size effect on the ionic activation energy.

EXPERIMENT

The $MAPbI_3$ thin film was fabricated by spin-coating of $MAPbI_3$ precursor either on glass or FTO coated glass depending on the type of experiments. The film was deposited using anti-solvent method that includes three steps of spin-coating with speeds of 500, 3500, and 5000 rpm for 3, 10, and 30 seconds, respectively [11]. For obtaining shiny and continuous film, 600 μL of toluene, used as an anti-solvent, was dropped 4 seconds before start of the 3rd step. The samples were annealed at 100º C for 10 minutes immediately after the spin-coating. Finally, 60 nm Au

was deposited on $MAPbI_3$ for metal contact. For various types of characterizations, x-ray diffraction (XRD), impedance spectroscopy (IS), LCR (inductance-capacitance-resistance) meter, spectrophotometer, and conductive AFM (c-AFM) were used. Different temperature dependent measurements were carried out using a thermo-electric generator with calibrated temperature sensor with an accuracy of ± 1 °C.

DISCUSSION

The reported transition temperature of tetragonal to cubic phase for $MAPbI_3$ is scattered in a wide range [2]. Here we first determine the structural transition temperature for our typical spin-coated samples. As the Fig. 1 shows, (211) and (202) planes were selected for the temperature dependent XRD measurement. The (211) plane disappears in the cubic state, whereas the (202) plane in tetragonal structure evolves into the (111) cubic plane with a slight decrease in 2θ angle. From these (h, k, l) values lattice parameters of both tetragonal phase (a, and c), and cubic phase (a) can be determined by following equation based on the Bragg's law [12]:

$$\text{Tetragonal: } 1/d^2 = (h^2 + k^2)/a^2 + l^2 / c^2, \text{ Cubic: } 1/d^2 = (h^2 + k^2 + l^2) / a^2 \quad (1)$$

Where d is the lattice plane spacing. To find the phase transition temperature, the lattice parameters of both phases can be related vis following equations [13]:

$$a^* = a/\sqrt{2},\ c^* = c/2,\ d = V^{1/3}, \text{ and for fitting: } a^* \text{ (or } c^*) = d + m(T_c - T)^{\beta} \quad (2)$$

Where a^*, and c^* are modified lattice constants in tetragonal phase along a and c axes respectively, d is the equivalent lattice parameter in tetragonal phase comparing to cubic phase, V is unit cell volume, as shown in Fig. 1(b).

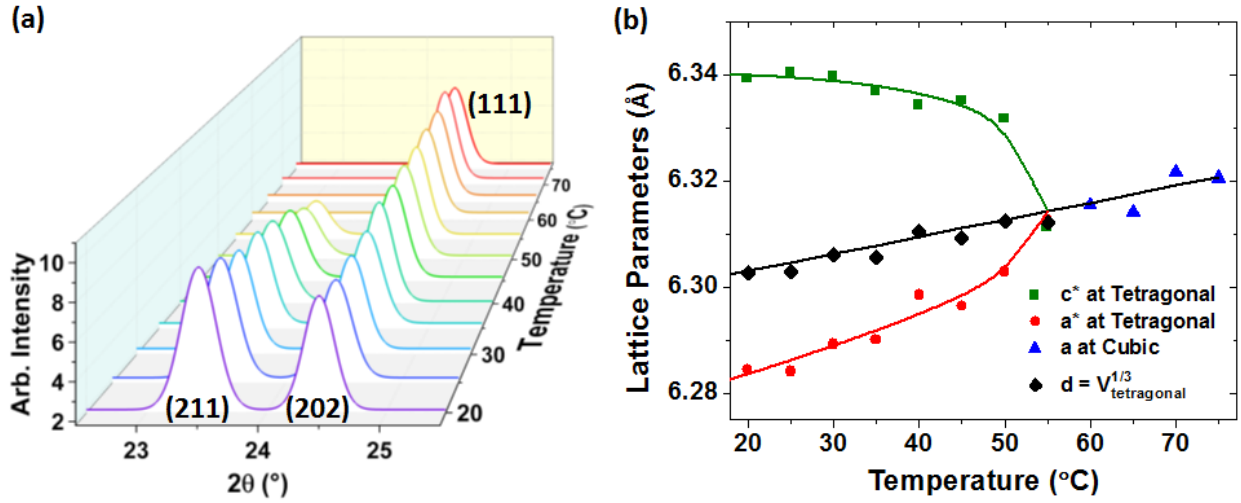

Figure 1. (a) XRD scan of $MAPbI_3$ sample at different temperatures showing the change of (211), and (202) planes with temperature. (b) Lattice parameters extracted from the XRD data of (a) showing the tetragonal to cubic transition temperature as ~ 55 °C.

Finally, a^* and c^* can be fitted by equation 2 where m, and β are fitting parameters. As the temperature is increased, the lattice parameter a increases, and c decreases in tetragonal phase. Eventually, the phase transition temperature can be determined at which both parameters evolve to be equal as parameter a of cubic structure. From Fig. 1(b) we have found this temperature for our sample as ~55 °C. Figure 1 further indicates that the crystal symmetry transition of $MAPbI_3$ perovskite occurs in a continuous mode with a "soft" transition nature.

Impedance spectra were taken for a FTO/$MAPbI_3$/Au sandwich structure at different temperatures under dark condition to characterize the intrinsic ionic migration properties of the material. The Warburg diffusion was particularly considered when selecting the model to fit the spectra. More detail can be found from Ref. [8]. The Bode plot was extracted from the IS data as shown in Fig. 2(a), which shows that the characteristic frequency (f_0) of ionic transportation in a hopping process shifts towards higher frequency as the temperature is increased. Ionic migration activation energy can be calculated from the following equations:

$$\tau = 1/2\pi f_0, \text{ and } k = 1/\tau \tag{3}$$

Where τ represents the relaxation time constant, and k represents the ion hopping rate constant. Using the k values in Arrhenius plot, we can determine the ionic migration activation energy as shown in Fig. 2(b). From here, two different temperature regions are observed with a boundary at ~ 45 °C, below which the activation energy is ~ 0.7 eV, while it is ~ 0.5 eV above this temperature. The two different activation energy might be attributed to the different phases of $MAPbI_3$. However, this temperature is clearly 10 °C less than the tetragonal-cubic transition temperature determined from the XRD study.

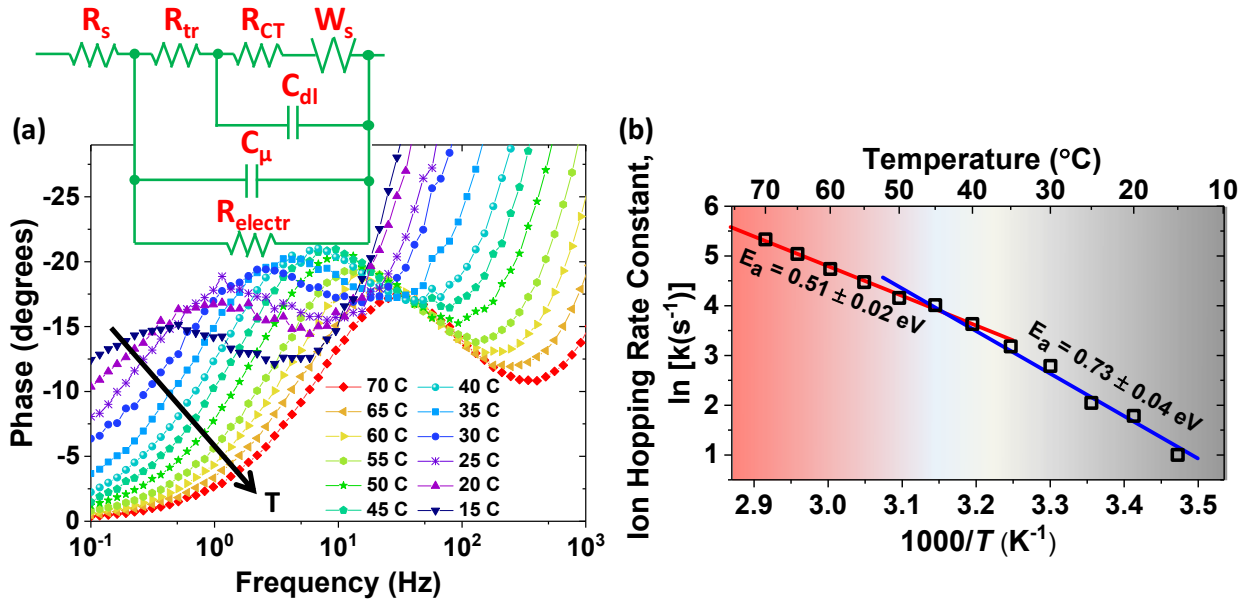

Figure 2. (a) The Bode plot from impedance spectroscopy for FTO/$MAPbI_3$/Au sandwich structure at different temperatures. Inset shows the equivalent circuit model. (b) The Arrhenius plot of the ion hopping rates obtained from the Bode plot showing different activation energies below and above ~45 °C.

The ion activation energy, temperature-dependent ion conductivity, ionic diffusion coefficient, and ionic mobility were further derived by using the circuit model in the inset of Fig.

2(a) to fit the Nyquist plot of IS spectra. In this model, R_{CT} represents the interfacial charge transfer resistance at contacts, C_{dl} as double-layer capacitance due to ionic blocking at the contact, W_s as Warburg element, and R_{tr} as coupled electron and ion transport resistance. In addition, R_{electr} represents free carrier recombination or transport that is not coupled to ion diffusion/accumulation, R_s as series contact resistance, C_μ as chemical capacitance of the perovskite layer. Two activation energies with value of ~ 0.7 eV and ~ 0.5 eV were found intersecting at ~ 45 °C. From 15 ºC to 70 ºC, ion diffusion coefficient was found varying from $6.5\text{x}10^{-10}$ to $5\text{x}10^{-8}$ cm^2s^{-1}, and mobility changing between $2.6\text{x}10^{-7}$ and $1.7\text{x}10^{-5}$ $cm^2V^{-1}s^{-1}$. Particularly at room temperature, their values were found to be $2.0\text{x}10^{-9}$ cm^2s^{-1} and $7.6\text{x}10^{-7}$ $cm^2V^{-1}s^{-1}$, respectively.

Capacitance spectra is another tool for measuring the dielectric characteristics across the tetragonal to cubic phase transition. Using a LCR meter, *C-f* curves were obtained at different temperatures under dark condition, as shown in Fig. 3(a). The dielectric constant (ε'), which depends on the temperature, can be derived from the capacitance. At lower frequencies, the dielectric constant has a larger value at higher temperatures, whereas the trend becomes opposite at frequencies over 1,000 Hz. This is clearer in Fig 3(b), where the dependence of the dielectric constant on temperature at three different frequencies of 100 Hz, 1,000 Hz, and 10,000 Hz are shown. Interestingly, in all three cases the transition occurs closely at ~ 45 °C again, validating the ionic migration trend found in IS study of Fig. 2.

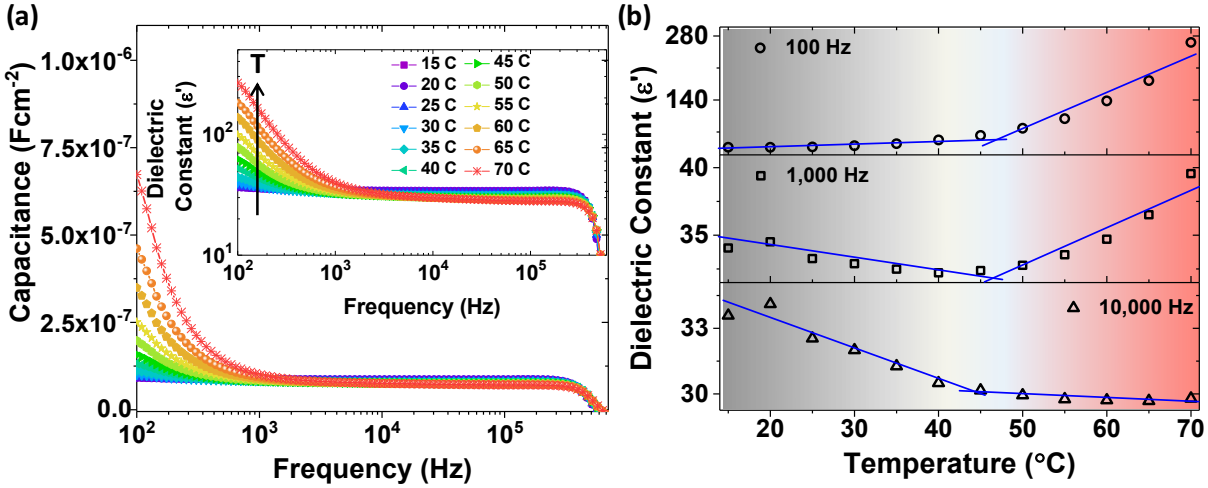

Figure 3. (a) Temperature dependent capacitance spectra for FTO/$MAPbI_3$/Au sandwich structure at different temperatures. The inset shows dielectric constant (ε') deduced from the capacitance spectra. (b) Dielectric constant (ε') at three representative frequencies for different temperatures showing two different trends with a boundary at ~ 45 °C.

From these electrical studies, we found that although ion energy barrier change in $MAPbI_3$ is related to crystal symmetry, it does not necessarily occur at the same temperature as the tetragonal-cubic structural phase transition. This discrepancy might be explained by the continuous nature of $MAPbI_3$ perovskite crystal symmetry transition and the strong instantaneous deviation from the cubic symmetry at high temperature.

It has previously been shown that the optically determined band gap of $MAPbI_3$ does not change abruptly from tetragonal to cubic phase due to monotonic blue-shift with temperature along with the fact that the cubic structure goes through deviation in picosecond scale, which is

much smaller than the time scale for electronic or ionic transitions [14]. Indeed, our sample showed that there is no clear transition pattern from the bandgap of $MAPbI_3$ at different temperatures obtained by Tauc plot as shown in Fig. 4. This monotonous increase of bandgap with temperature can be explained by the lowering of the valence band maximum with increasing temperature. Thus, different transition temperatures from different measurements are validated.

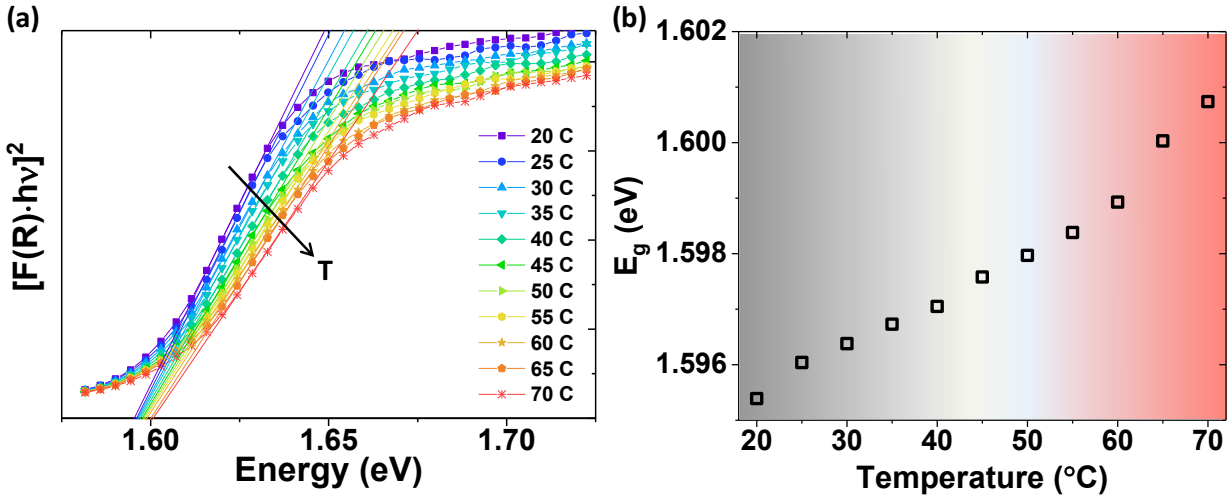

Figure 4. (a) Plot of $[F(R)\cdot h\nu]^2$ versus photon energy ($h\nu$) at different temperatures. (b) Band gap at different temperatures measured from the Tauc plot shown in (a).

Finally, we selected three samples with different grain sizes for the ionic migration study in the temperature range of interest. To do so, different grain sized samples were fabricated by changing the precursor concentration, annealing temperature, and annealing atmosphere. Then, following the experiment shown in Fig. 2 activation energy for ion hopping in $MAPbI_3$ was determined for three different samples. Not shown here, there was a clear trend in increment of ionic activation energy with increment of grain sizes. The grain boundaries have significant effect in enhancing the ionic transport of perovskites acting as shortcut path for movement of ions comparing to the inside of the grain. Since, grain boundary density (length of total grain boundaries in a unit area) for smaller grained sample is larger than that of larger grained sample, ionic activation energy is smaller for smaller grained sample.

To further investigate the ionic conduction, we have done c-AFM on the grain boundary of a $MAPbI_3$ film surface at different temperatures with or without light illumination. As the temperature is increased the current increased drastically. Similar behavior was observed for the hysteresis. This is true for both dark and light conditions, showing the inherent ionic migration properties of $MAPbI_3$, which is prominent in the grain boundary. It was further observed that the photon could significantly enhance the ionic migration [15], which is apparent from almost one order increase in current in the grain boundary under light illumination.

CONCLUSIONS

In summary, we conducted structural, electrical/ionic, and optical property studies of $MAPbI_3$ thin films in normal solar cell operation temperature up to 70 °C. Temperature dependent crystal structure study revealed that the tetragonal to cubic phase transition occurred

at ~55 °C for these samples. The changing rate of ionic/electrical properties had an abrupt transition across a temperature of ~45 °C due to the abrupt change of ion activation energy. Although ion energy barrier change in $MAPbI_3$ is related to crystal symmetry, it does not necessarily occur at the same temperature as the tetragonal-cubic structural phase transition. This discrepancy might be explained by the continuous nature of $MAPbI_3$ perovskite crystal symmetry transition and the strong instantaneous deviation from the cubic symmetry at high temperature. Optical absorption measurement and temperature dependent bandgap study indicated that there was no clear transition from optical properties. Finally, from ionic conduction measurement for different grain sizes, it was found that the activation energy for ionic migration is higher for larger grain size, almost 3 times higher when the average grain size was increased from ~ 0.26 μm to 1.40 μm. Thus, to prevent ionic migration in the perovskite solar cell, $MAPbI_3$ films with larger grain sized should be targeted.

ACKNOWLEDGMENTS

Funding for the work at Texas Tech University from the National Science Foundation (CBET-1438681) is greatly acknowledged.

REFERENCES

1. D. Li, P. Liao, X. Shai, W. Huang, S. Liu, H. Li, Y. Shen and M. Wang, *RSC Adv.* **6** (92), 89356-89366 (2016).
2. R. L. Milot, G. E. Eperon, H. J. Snaith, M. B. Johnston and L. M. Herz, *Adv. Funct. Mater.* **25** (39), 6218-6227 (2015).
3. T. Hata, G. Giorgi and K. Yamashita, *Nano Lett.* **16** (4), 2749-2753 (2016).
4. T. Y. Yang, G. Gregori, N. Pellet, M. Grätzel and J. Maier, *Angew. Chem.* **127** (27), 8016-8021 (2015).
5. S. Meloni, T. Moehl, W. Tress, M. Franckevičius, M. Saliba, Y. H. Lee, P. Gao, M. K. Nazeeruddin, S. M. Zakeeruddin and U. Rothlisberger, *Nat. Commun.* **7**, 10334 (2016).
6. M. Bag, L. A. Renna, R. Adhikari, S. Karak, F. Liu, P. M. Lahti, T. P. Russell, M. T. Tuominen and D. Venkataraman, *J. Am. Chem. Soc.* **137** (40), 13130–13137 (2015).
7. M. N. F. Hoque, M. Yang, Z. Li, N. Islam, X. Pan, K. Zhu and Z. Fan, *ACS Energy Lett.* **1** (1), 142-149 (2016).
8. M. N. F. Hoque, N. Islam, Z. Li, G. Ren, K. Zhu and Z. Fan, *ChemSusChem* **9** (18), 2692-2698 (2016).
9. J. S. Yun, A. Ho-Baillie, S. Huang, S. H. Woo, Y. Heo, J. Seidel, F. Huang, Y.-B. Cheng and M. A. Green, *J. Phys. Chem. Lett.* **6** (5), 875-880 (2015).
10. Y. Shao, Y. Fang, T. Li, Q. Wang, Q. Dong, Y. Deng, Y. Yuan, H. Wei, M. Wang and A. Gruverman, *Energy Environ. Sci.* **9** (5), 1752-1759 (2016).
11. N. Islam, M. Yang, K. Zhu and Z. Fan, *J Mater. Chem. A* **3** (48), 24315-24321 (2015).
12. T. J. Jacobsson, L. J. Schwan, M. Ottosson, A. Hagfeldt and T. Edvinsson, *Inorg. Chem.* **54** (22), 10678-10685 (2015).
13. Y. Kawamura, H. Mashiyama and K. Hasebe, *J. Phys. Soc. Jpn* **71** (7), 1694-1697 (2002).
14. C. Quarti, E. Mosconi, J. M. Ball, V. D'Innocenzo, C. Tao, S. Pathak, H. J. Snaith, A. Petrozza and F. De Angelis, *Energy Environ. Sci.* **9** (1), 155-163 (2016).
15. J. Xing, Q. Wang, Q. Dong, Y. Yuan, Y. Fang and J. Huang, *Phys. Chem. Chem. Phys.* **18** (44), 30484-30490 (2016).